DETERMINATION OF MS TEMPERATURE IN STEELS. A BAYESIAN NEURAL NETWORK MODEL.

C. CAPDEVILA, F. G. CABALLERO, and C. GARCÍA DE ANDRÉS

Dr. C. Capdevila and Dr. F. G. Caballero, Post-doctoral Research Assistants, and Dr. C. García de Andrés, Research Scientist, are in the Department of Physical Metallurgy, Centro Nacional de Investigaciones Metalúrgicas (CENIM), CSIC, Avda. Gregorio del Amo, 8, 28040 Madrid, Spain.

Abstract

The knowledge of the martensite start (Ms) temperature of steels is sometimes important during parts and structures fabrication, and it can not be always properly estimated using conventional empirical methods. The additions in newly developed steels of alloying elements not considered in the empirical relationships, or with compositions out of the bounds used to formulate the equations, are common problems to be solved by experimental trial and error. If the trial process was minimised, cost and time might be saved. This work outlines the use of an artificial neural network to model the calculation of Ms temperature in engineering steels from their chemical composition. Moreover, a physical interpretation of the results is presented.

KEY WORDS: Neural Network Analysis; Martensite; Modelling Phase Transformation; Steels

1. Introduction

The Ms temperature is of vital importance for engineering steels. Hence great efforts have been made in predicting the Ms temperature of these steels. Obviously, chemical composition of steel is the main factor affecting its Ms although the austenitising state, external stresses and stored deformation energy may sometimes play and important role as well. Martensite start temperatures are usually relatively easy to calculate as long as the steels have a low alloy content [1-6]. Even though empirical equations exists for high alloy steels, they are not sufficiently general and are known to provide inaccurate answers for the new steels which contain different alloying elements, or their compositional range are out of bounds of those used to formulate the equations.

For instance, the interest of copper additions to the chemical composition of steels has increase in the last years. Copper-bearing low carbon steels are used in heavy engineering applications which demand a combinations of strength, toughness and weldability [7-11]. Strength is achieved by precipitation of fine copper precipitates during ageing, instead of precipitation of carbide particles [12]. Therefore, copper is not in this respect different from any secondary hardening element in steels. Likewise, it has been demonstrated that copper sulphide strongly enhance acicular ferrite formation, which induces a good combination of mechanical properties as compared to bainite and especially to ferrite-pearlite microstructures [13-15].

Likewise, power stations are nowadays designated to operate with steam temperatures in excess of 873 K. The steels currently being developed to cope with these requirements contain a total solute concentration which is often in excess of 14 wt.-%. The main solutes include carbide forming elements such as chromium and molybdenum. Chromium also provides the necessary corrosion and oxidation resistance for prolonged elevated temperature service. The main alloys under consideration include numerous variants of the classical 12Cr-

1Mo and 9Cr-1Mo steels [16-17]. These alloys have a high hardenability and a microstructure which is predominantly martensitic on cooling from the austenitising temperature. Their martensitic start Ms temperature is therefore of considerable importance in deciding on the exact welding conditions necessary to avoid cracking [17]. An important variant of the 9Cr-1Mo steel is that in which tungsten is added to induce precipitation hardening [18].

Gustafson and Agren [19] reported that Co has a remarkable influence on coarsening of $M_{23}C_6$ carbides in the 9Cr-1Mo steel. Their results show that a final average radius of the carbides after 30 000 h at 873 K decreases in 30 % with a Co addition of 10 mass %. This raises the Orowan stress with 30 %. Moreover, it is assumed that slower particle coarsening also leads to a retard in the coarsening of the martensite lath structure. Thus, an improvement on creep life of the steels is expected [19].

Likewise, it has been reported that the combined additions of cobalt and tungsten to the chemical composition strengthen the steel by precipitation of tungsten-cobalt (WC-Co) cemented carbides [20]. These new steels are widely used as tool steels where a good combination between abrasion resistance and corrosion resistance is required [21-23].

It is then followed that the investigation of how copper, tungsten, and cobalt additions may affect the Ms temperature is an important issue. Thus, the aim of this work is to develop an artificial neural network model to predict the Ms temperature of steels and to understand the influence of the chemical composition on this temperature. Neural networks are of use whenever the intricacy of the problem is overwhelming from a fundamental perspective and where simplification is unacceptable. They represent a powerful method of non-linear regression modelling. The present knowledge on the role of elements such as carbon, manganese, molybdenum, chromium, nickel and silicon in the formation of martensite was taking into account in this modelling, and new elements such as copper, tungsten, and cobalt have been also included in calculations.

2. The experimental database

The definition of the Ms temperature in any model ideally requires a complete description of the chemical composition. A search of the literature [24-29] allowed us to collect 748 individual examples where the chemical composition and Ms values were reported in detail. Table l shows the 14 input variables used for the analysis of Ms temperature.

It was possible to find 670 cases where all of these variables were reported except for nitrogen content. It would be unreasonable to set nitrogen content to zero when its value is not reported since steels inevitably contain this impurity element in practice. Therefore, when the nitrogen content was missing its concentration was set to the mean value calculated for the 748 cases of the database. For other elements such as Mn, Ni, etc, their contents were set to zero when they were not reported. This is a reasonable procedure since they would not then be deliberate added or their concentrations were close to the limits of the chemical analysis techniques.

3. Brief description of neural network

Neural network analysis has been applied to estimate the Ms temperature as a function of the variables listed in Table 1. It is a general method of regression which it can be at first explained by using the familiar linear regression method. Chemical composition of each alloy element (x_i) define the inputs nodes, and the martensite start temperature the output node. Each input is multiplied by a random weight w_i and the products are summed together with a constant θ to give the output node $y = \sum_i w_i x_i + \theta$. The weights are systematically changed until a best fit description of the output is obtained as a function of the inputs. This operation is known as training the network.

The network can be non-linear. As before, the input with data x_j are multiplied by weights ($w_j^{(1)}$), but the sum of all these products forms the argument of a hyperbolic tangent (tanh):

$$h = tanh\left(\sum_j w_j^{(1)} x_j + \theta_j^{(1)}\right)$$
$$y = w^{(2)} h + \theta^{(2)} \quad (2)$$

where $w^{(2)}$ is a weight and $\theta^{(2)}$ another constant. The output y is therefore a non-linear function of x_j. The function usually chosen being the hyperbolic tangent because of its flexibility [30-31]. The exact shape of the hyperbolic tangent can be varied by altering the weights w_j.

A one hidden-unit model may not however be sufficiently flexible. Further degrees of non-linearity can be introduced by combining several of the hyperbolic tangents, permitting the neural network method to capture almost arbitrarily non-linear relationships. The number of tanh functions is the number of hidden units. The function for a network of i hidden units is given by

$$y = \sum_i w_i^{(2)} h_i + \theta^{(2)} \quad (3)$$

where

$$h_i = tanh\left(\sum_j w_{ij}^{(1)} + \theta_i^{(1)}\right) \quad (4)$$

Notice that the complexity of the function is related to the number of hidden units. The availability of a sufficiently complex and flexible function means that the analysis is not as restricted as in linear regression where the form of the equation has to be specified before the analysis. Figure 1(a) shows that as expected the inferred noise level of data (σ_v) decreases monotonically as the number of hidden units increases. However, the complexity of the model also increases with the number of hidden units. A high degree of complexity may not be justified if the model attempts to fit the noise in the experimental data. To find out the optimum number of hidden units of the model the following procedure was used. The

experimental data were partitioned equally and randomly into a test dataset and a training dataset. Only the latter was used to train the model, whose ability to generalist was examined by checking its performance on the unseen test data. The test error (T_{en}) is a reflection of the ability of the model to predict the Ms values in the test data:

$$T_{en} = 0.5\sum_{n}\left(y_n - t_n\right)^2 \tag{5}$$

where y_n is the set of predictions made by the model and t_n is the set of target (experimental) values. In Fig. 1(b), it can be seen that the calculated test error for this Ms model goes through a minimum at 1 hidden unit. Therefore, the optimum model is that which considers only one hidden unit.

However, it is possible that a *committee* of models can make a more reliable prediction than an individual model. The best models were ranked using the values of their test errors as Fig. 2(a) presents. Committee of models could then be formed by combining the prediction of the best L models, where L = l ,2,... The size of the committee is therefore given by the value of L.

The test error of the predictions made by a committee of L models, ranked 1 ,2...q...L, each with n lines of test data, is calculated in a similar manner to the test error of a single model:

$$\begin{aligned} T_{en} &= 0.5\sum_{n}\left(\overline{y_n} - t_n\right)^2 \\ \overline{y}_n &= \frac{1}{L}\sum_{q} y_n^{(q)} \end{aligned} \tag{6}$$

The test error of the committee as a function of the models considered is plotted in Fig. 2(b). It is seen that the test error goes through a minimum for the committee made up of seven models. Therefore, the neural network model used to calculate the Ms temperature in this paper is a committee of seven models.

From a comparison between Fig. 1(b) and Fig. 2(b) it is clear a reduction in test error and hence improved predictions by using the committee model approach. Comparison between

the predicted and measured values of Ms for the training and test data is shown in Figs. 3 for the best committee (consisting of seven best models).

However, the practice of using a best-fit function does not adequately describe the uncertainties in regions of the input space where data are spare or noisy. MacKay [32-33)] has developed a particularly useful treatment of neural networks in a Bayesian framework, which allows the calculation of error bars representing the uncertainty in the fitting parameters. The method recognises that there are many functions which can be fitted or extrapolated into uncertain regions of the input space, without unduly compromising the fit in adjacent regions which are rich in accurate data. Instead of calculating a unique set of weights, a probability distribution of sets of weights is used to define the fitting uncertainty. The error bars therefore become larger when data are spare or locally noisy.

4. Influence of carbon

Undoubtedly, carbon plays the strongest role in decreasing the Ms temperature. The phenomenological influence of carbon upon the Ms temperature is shown in Fig. 4. The decrease rate of Ms temperature reduces when the carbon concentration in the alloy increases, which is implied by the decrease in the slope of the Ms-C (wt.- %) line. This result is consistent with experimental observations carried out by Eichelman and Hull [34)] which reported that a very low carbon concentration, where C-X interactions are very weak, the carbon-influencing factor tends to increase. However, as carbon concentration increases, the influence of binary interactions becomes more important and then the influence of carbon itself on Ms temperature decreases.

5. Influence of substitutional alloying elements

The main advantage of the neural network model as compared with other empirical models is the ability of analysing separately the influence on Ms temperature of each of the alloying elements. In this sense, the role of alloying elements such as Cr, Co, Mo, Si, Mn, Ni, Cu and W on Ms temperature has been analysed in this section.

The alloying elements may be grouped into two categories. Those which expand the γ–field and encourage the formation of austenite over a wider compositional limits or γ-stabilisers (*i.e.*, Mn, Ni and Cu), and those which contract the γ–field and encourage the formation of ferrite over a wider compositional limits of α–stabilisers (*i.e.*, Cr, Co, Mo, Si and W).

Figure 5 shows the influence of the γ–stabilisers alloying elements on Ms temperature for three different grades of carbon. It is clear from Fig. 5(a) and 5(b) that Mn and Ni are the elements which have the major influence on Ms after carbon. Likewise, the small error bars indicate that there is a low dispersion in the database and the number of data considered is enough to reduce the uncertainty in the predictions to the minimum.

Nevertheless, the effect of the Cu on Ms is not as clear as the γ-stabiliser elements analysed above. Fig. 5(c) suggests that for copper concentrations up to 1 wt.-% this element does not influence on Ms temperature although the increase in error bars indicates a lack of data for high copper concentrations.

Figure 6 shows the influence of α–stabilisers elements such as Co, W, Mo, Si and Cr for three different grades of carbon. It has been experimentally demonstrated the influence of cobalt promoting the formation of bainite in detriment of martensite in Fe-Cr-C weld deposits [35]. This indicates that cobalt (in concentrations lower than 1 wt.-%) is a potentially good alloy element to develop a fully bainitic high strength steel. Likewise, large amount of cobalt (≈19 wt.-%) is added to promote the precipitation of strong W-Co carbides in tool steels 20). It is

suggested from Fig. 6(a) that cobalt concentrations lower than 3 wt.-% does not affect Ms temperature. However, for cobalt concentration between 3 and 30 wt.-% (that used when WC-Co carbides are formed), the higher cobalt content, the higher Ms temperature.

An important variant of the 9Cr-1Mo power plant steel is that in which tungsten is added to induce precipitation hardening. Since Ms temperature is of considerable importance in deciding on the exact welding conditions necessary to avoid cracking in these steels, it is necessary to study the influence of tungsten on Ms temperature. It is clear from Fig. 6(b) that tungsten increases the value of Ms for the three different grades of carbon analysed. However, the neural network predictions are in contrast to some experimental results which reveals that the addition of large concentration of tungsten (up to 3 wt.-%) to the 9Cr-1Mo power plant steel drops the Ms temperature [36-37]. Further investigations revealed that the cause of this contradiction may be due to the presence of δ ferrite at the austenitising temperature selected (a temperature of 1373 K) 36). It is therefore not surprising that the neural network predicting Ms temperature does not agree with that measured in this 9Cr-1Mo power plant steels. Moreover, Figs. 6(c) and 6(d) show the influence of Mo and Si upon the Ms temperature, respectively. It is clear from these figures that molybdenum and silicon have opposite effects on Ms temperature. Molybdenum slightly increase Ms, whereas silicon decreases Ms temperature.

It is possible to get a physical understanding of these results. According to their chemical properties, molybdenum and tungsten can be classified as strong carbide former meanwhile silicon is a non-carbide former. This behaviour may be attributed to the influence of alloying elements on the activity of carbon in the solid solution. Keeping this in mind, we can expect that interactions between carbon and molybdenum or tungsten tend to weaken the role of carbon, and rise Ms. In this sense, large amount of cobalt promotes the formation of complex carbides [21] and then cobalt also may behave as a carbide former. Therefore, an increase of Ms

is expected. The interaction of carbon with non-carbide forming elements, such as silicon, may enhance the role of carbon, and lead to a further decrease in Ms.

On the other hand, although Cr is an intermediate carbide former element, this element always decreases the Ms temperature as shown in Fig. 6(e). This result is fully consistent with those reported in the literature demonstrating the role of chromium decreasing Ms temperature [38]. The small error bars in Fig. 6(e) indicate that this tendency it is well establish in the database and the scatter is very small. It is worthy to mention that although chromium is a weak α–stabiliser, its influence on Ms temperature is very strong. Actually, its effect on Ms is comparable to Mn and Ni which are γ–stabiliser elements.

It is clear from Figs. 5 and 6 that Cr, Ni, Co and W have different effects on Ms temperature. Figure 7 shows the influence on Ms of different combinations between such elements. Figures 7(a) and 7(b) suggest that the effect of Ni decreasing Ms is stronger than the raise produced by an increase in tungsten or cobalt concentrations. In this sense, Fig. 7(c) shows that tungsten additions are not able to compensate for the effect of chromium decreasing Ms. However, Fig. 7(d) suggests that the additions of cobalt changes the tendency of Ms temperature depending on the chromium concentration. At chromium contents lower than 9 wt.-%, cobalt additions rise Ms temperature. However, chromium concentrations higher than 9 wt.-%, the addition of cobalt causes a decrease in Ms temperature.

6. Thermodynamic validation of neural network results

In this section, a thermodynamic explanation to the presented neural networks results is discussed. The thermodynamic calculations involved here have been performed using the commercial software package, MTDATA [39]. The two sublattice model [40] was used to express the Gibbs free energies of ferrite and austenite phases. The first sublattice is occupied

by substitutional atoms and the second is occupied by interstitial atoms and vacancies. The Gibbs free energies of austenite, G^{γ}, and ferrite of the same composition, G^{α}, were calculated separately by allowing only one phase to exist in the system. Then, the molar Gibbs free energy difference, $\Delta G^{\gamma\alpha} = G^{\alpha} - G^{\gamma}$, at different temperatures was obtained. The Gibbs free energies of both phases include unitary terms of free energies, mixing entropies, excess free energies describing the deviation from the regular solution model, and magnetic contributions. However, to calculate the driving force for martensite transformation ($\Delta G^{\gamma\alpha'}$) also requires an estimation of the Zener ordering energy [41], since carbon atoms in ferrite can in some circumstances order on one of available sublattices of octahedral interstitial sites, thereby changing the symmetry of the lattice from bcc to bct. The ordering temperature, T_c, is a function of the carbon concentration [42]. If the Ms temperature exceeds T_c, then the martensite is bcc, but when it is below T_c, martensite is bct. The ordering energy is a complicated function of temperature and carbon concentration, and was calculated as in Ref. 42). The required free energy is then given by $\Delta G^{\gamma\alpha'} = \Delta G^{\gamma\alpha} + G_{Zener}$.

In the thermodynamic approach, martensite is said to be triggered when the chemical driving force ($\Delta G^{\gamma\alpha'}$) achieves some critical value at the Ms temperature ($\Delta G_C^{\gamma\alpha'}$). Bhadeshia [43,44] evaluated $\Delta G_C^{\gamma\alpha'}$ for low alloy steels using the Lacher, Fowler and Guggenheim method [45,46] together with relatively accurate thermodynamic data. He concluded that $\Delta G_C^{\gamma\alpha'}$ varies between –900 to –1400 J mol^{-1} as a function of the carbon content. The presence of alloying elements is acknowledged by allowing for their effects on the magnetic and non-magnetic components of the free energy change accompanying the γ–α transformation in pure iron. Additionally, the carbon-alloying element interaction is taken into account by suitably modified the C–X pair interaction energy.

However, this method does not work well when it is applied to high alloyed steels. Cool and Bhadeshia [36] proposed a new model to calculate $\Delta G_C^{\gamma\alpha'}$ which can be applied to the determination of the Ms temperature of highly alloyed steels. The model is based in the Ghosh and Olson [24] method which takes into consideration the strengthening of austenite caused by solute additions. Ghosh and Olson proposed that the critical martensite driving force is the addition of two terms. The former includes strain and interfacial energies, and the latter is the interfacial frictional work between the austenite matrix and martensite nucleus which is composition dependent. The critical value in J mol^{-1} of the driving force needed to trigger martensitic transformation is:

$$-\Delta G_C^{\gamma\alpha'} = 683 + 4009c_C^{0.5} + 1879c_{Si}^{0.5} + 1980c_{Mn}^{0.5} + 172c_C^{0.5} + 1418c_{Mo}^{0.5} + 1868c_{Cr}^{0.5} + 1618c_V^{0.5} + 752c_{Cu}^{0.5} + 714c_W^{0.5} + 1653c_{Nb}^{0.5} + 3097c_N^{0.5} - 352c_{Co}^{0.5} \quad (7)$$

where $c_i^{0.5}$ are the square root of the different alloying elements concentration in mole fraction. The coefficients were obtained by Ghosh and Olson by establishing the $c_i^{0.5}$ dependence and fitting over a wide range of compositions: the maximum concentrations were approximately 2 wt.-% for carbon and nitrogen, 0.9 wt.-% vanadium and about 2-28 wt.-% for all the other alloying elements [47]

Figure 8 shows the evolution of $\Delta G^{\gamma\alpha'}$ for different grades of Mn, Ni and Cu maintaining a constant concentration of carbon C=0.4 wt.-%. Superimposed to this calculations it is shown the corresponding calculated values of $\Delta G_C^{\gamma\alpha'}$ according to Cool and Bhadeshia model. It is clear that all the γ-stabiliser elements analysed reduces (in absolute value) $\Delta G^{\gamma\alpha'}$, and therefore Ms temperature is reduced. Also, it is concluded form Figs. 8(a) and 8(b) that the effect of Mn and Ni is more pronounced that the effect of Cu, which is negligible (Fig. 8(c)). These results are consistent with those predicted by the neural network model presented above. Likewise, it is followed from these figures that the effect of Mn and Ni is quite different. Meanwhile Ni addition considerably reduces the value of $\Delta G^{\gamma\alpha'}$ and hardly changes

the value of $\Delta G_C^{\gamma\alpha'}$, the effect of Mn addition is more pronounced increasing $\Delta G_C^{\gamma\alpha'}$ that decreasing $\Delta G^{\gamma\alpha'}$.

Figure 9 shows the evolution of $\Delta G^{\gamma\alpha'}$ for different grades of Co, W, Cr, Si and Mo, maintaining a constant concentration of carbon C=0.4 wt.-%. It is suggested from Figs. 9(a) and 9(b) that cobalt and tungsten addition increases the Ms temperature, as the neural network predicted. Likewise, the addition of chromium and silicon drops Ms temperature (Figs. 9(c) and 9(d)). On the other hand, molybdenum addition hardly affects the chemical driving force for martensite transformation. Moreover, its effect on the value of $\Delta G_C^{\gamma\alpha'}$ is almost negligible leading to a slightly decreases in Ms temperature (Fig. 9(e)). It could be then concluded that molybdenum does not have a sensible effect on Ms temperature, which is consistent with the predictions of the neural network analysis.

Finally, Fig. 10 shows the combined effect of cobalt and chromium on Ms temperature. It is followed from the Fig. 10(a) that concentration values of Co=12 and Cr=0 wt.-% increase Ms temperature as compared with Co=0 and Cr=0 wt.-%, as it was expected considering the influence of Co presented in Fig. 6(a) and 9(a). However, Fig. 10(b) shows that the combined addition of Co=12 and Cr=15 wt.-% decreases the Ms temperature at values even lower that those obtained for concentrations of Co=0 and Cr=15 wt.-%. This result is in accordance with the neural network prediction.

7. Use of the model

7.1. New empirical relationship describing the effect of steel chemistry

It is well known that Ms of a steel can be estimated by statistical formulas in the general form of

$$Ms = k_o + \sum k_i w_i \quad (8)$$

k_o is the offset parameter, i indicates the alloying element, w_i stands for the concentration (wt.- %) of element i, and k_i is its corresponding linear coefficient. The relationship between the martensite start transformation and steel composition has been investigated by Grange and Stewart [3], Payson and Savage [4],Kung and Rayment [5], and Andrews [6]. Andrews used the largest number of samples and he reported the following linear relationship:

$$M_s(^oC) = 539 - 423w_C - 30.4w_{Mn} - 17.7w_{Ni} - 12.1w_{Cr} - 7.5w_{Mo} \quad (9)$$

In order to find out a similar linear dependence of the Ms upon the chemical composition, the results from the neural network analysis for Ms temperature were plotted by pairs of elements (C-Mn, C-Ni, C-Cu, C-W, C-Co, C-Cr, and C-Mo). Thus, Fig. 11 shows the evolution of Ms as carbon and chromium concentrations are varying from 0.001 to 0.9 wt.%, and from 0 to 17 wt.-%, respectively. These values are fitted to a plane regression equation ($M_s = y_o + ax + by$, where x correspond to carbon concentration values in wt.-%, and y correspond to the alloying element) by non-linear regression analysis. The regression coefficients a and b for the different alloying elements are listed in Table 2. R in Table 2 is the correlation factor between the neural network data and the parameters of the $M_s = y_o + ax + by$ fitting equation.

Therefore, the relative effect of other alloying elements is indicated in the following empirical relationship obtained from the neural network analysis

$$\begin{aligned} M_s(K) = {} & 764.2 - 302.6w_C - 30.6w_{Mn} - 16.6w_{Ni} - 8.9w_{Cr} + 2.4w_{Mo} \\ & - 11.3w_{Cu} + 8.58w_{Co} + 7.4w_W - 14.5w_{Si} \end{aligned} \quad (10)$$

7.2. Comparison with other Ms models

In this section we compare the neural network model predictions with the Cool and Bhadeshia 36) thermodynamic model. Likewise, a comparison is made between the predictions carried out by the Andrews' empirical equation (equation (9)), and that made by the relationship derived above (equation (10)). This analysis is performed in six very different alloys whose actual compositions are listed in Table 3. S1 is a commercial martensitic stainless steel, S2 is a high carbon high strength steel, S3 is a low carbon HSLA steel, S4 is a medium carbon forging steel, S5 and S6 are both power plant ferritic steels. All of these steels are used for commercial purposes, and therefore, the Ms temperature is a critical parameter whose accurate determination is very important in the processing route of the steel.

Figure 12 shows a comparison among the above mentioned models. It could be concluded from the figure that the neural network model presents the most accuracy on Ms temperature predictions.

8. Conclusions

1. A neural network method based within a Bayesian framework has been used to rationalise an enormous quantity of published experimental data on Ms temperature of steels. It is now possible, therefore, to estimate the Ms temperature as a function of the chemical compositions.
2. The formulated neural network model has been applied towards the understanding of the role of the most important alloying elements in commercial steels on the Ms temperature. This model predicts properly the role of well known alloying elements such as carbon, manganese, nickel, chromium, molybdenum and silicon. Likewise, the effect of elements such as copper, tungsten and cobalt whose use has recently increased due to the good

combination of mechanical properties induced in the steels has been also considered in this model.

3. An empirical equation similar to that formulated by Andrews [6] was presented. The influence of the alloying elements is considered by means of the C-X pair interactions. The results predicted by this equation among those predicted by the neural network model were compared with the experimental Ms temperature of six very different commercial steels. It is concluded that an excellent agreement between experimental and predicted Ms temperature was found.

Acknowledgements

The authors acknowledge financial support from Comisión Interministerial de Ciencia y Tecnología (PETRI 1995-0436-OP). F.G. Caballero would like to thank the Consejería de Educación, D.G. de Investigación de la Comunidad Autónoma de Madrid (CAM) for the financial support in the form of a Postdoctoral Research Grant. C. Capdevila would like to express his gratitude to the Consejo Superior de Investigaciones Cientifícas for financial support as a Post-Doctoral contract (I3P PC-2001-1).

References

1) L.A. Capella, *Metal. Prog*., **46**, (1944), 108.

2) J. Wang, P.J. van der Wolk and S. Van der Zwaag, *Mater. Trans*. JIM, **41**, 2000, 761-768.

3) R.A. Grange and HM. Stewart, *Trans. AIME*, **167**, (1946), 467.

4) P. Payson and H. Savage, *Trans ASM*, **33**, (1944), 261.

5) C.Y. Kung and J.J. Rayment, Hardenability Concepts with Applications to Steels, TMS-AIME, Warrendale, (1978), 229.

6) K.W. Andrews, *JISI*, **203**, (1965), 721.

7) E.V. Pereloma and J.D. Boyd, *Mater. Sci. Technol*., **12**, (1996), 1043.

8) G. Foularis, A.J. Baker and G.D. Papadimitriou, *Acta Mater*., **12**, (1996), 4791.

9) M.K. Banerjee, P.S. Banerjee and S. Datta, *ISIJ Int.*, **41**, (2001), 257.

10) S.W. Thompson, D.J. Colvin and G. Krauss,. *Metall. Trans*., **27A**, (1996), 1557.

11) C.N. Hsia and J.R. Yang, *Mater. Trans. JIM*, **41**, (2001), 1312.

12) R.A. Depaul and A.L. Kitchen, *Metall. Trans*., **1**, (1970), 389.

13) I. Madariaga, I. Gutierrez, C. Garcia de Andres and C. Capdevila, *Scripta Mater*., **41**, (1999), 229.

14) I. Madariaga and I. Gutierrez, *Acta Mater*., **47**, (1999), 951.

15) C. García de Andrés, C. Capdevila, I. Madariaga and I. Guitérrez, *Scripta Mater*., **45**, (2001), 709.

16) V.K. Sikka, C.T. Ward and K.C. Thomas, Ferritic steels for high temperature applications, ASM, Metals Park, (1983), 65.

17) P.J. Alberry and D.J. Gooch, *Weld. Met. Fabr*., **53**, (1985), 332.

18) F. Abe, *Mater. Sci. Eng*., **A319-321**, (2001), 770.

19) A. Gustafson and J. Agren, *ISIJ Int*., **41**, (2001), 356.

20) A.F. Lisovskii, *Powder Metall. Met. Ceram*., **39**, (2001), 428.

21) A.J. Gant and M.G. Gee, *Wear*, **250**, (2001), 908.

22) C.T. Kwok, F.T. Cheng and H.C. Man, *Surf. Coat. Technol*., **145**, (2001), 194.

23) C.T. Kwok, F.T. Cheng and H.C. Man, *Surf. Coat. Technol*., **145**, (2001), 206.

24) G. Gosh and G.B. Olson, *Acta Metall. Mater*., **42**, (1994), 3361.

25) M. Economopoulos, N. Lambert, and L. Habraken, Diagrames de transformation des aciers fabriques dans le Benelux, Centre National de Reserches Metakllurgiques, Bruxelles, (1967), 80.

26) M. Atkins, Atlas of continuous cooling transformation diagrams for engineering steels, British Steels Corporation, Sheffield, (1985), 17.

27) J. Wang, P. Van der Wolk and S. Van der Zwaag, *ISIJ Int*., **39**, (1999), 1038.

28) F.G. Caballero, H.K.D.H. Bhadeshia, K.J.A. Mawella, D.G. Jones and P. Brown, *Mater. Sci. Technol*., **17**, (2001), 517.

29) F.G. Caballero, H.K.D.H. Bhadeshia, K.J.A. Mawella, D.G. Jones and P. Brown, *Mater. Sci. Technol.*, **17**, (2001), 512.

30) D.J.C. Makay, *Neural Comput*., **4**, (1992), 698.

31) D.J.C. Makay, *Darwin college* J., (1993), 81.

32) D.J.C. Makay, *Neural Comput*., **4**, (1992), 415

33) D.J.C. Makay, *Neural Comput*., **4**, (1992), 448

34) G.H: Eichelman and F.C. Hull, *Trans ASM*, **45**, (1953), 77.

35) S.S. Babu, PhD Doctoral Thesis, University of Cambridge, Cambridge, (1991), 142.

36) T. Cool and H.K.D.H. Bhadeshia, *Mater. Sci. Technol*., **12**, (1996), 40.

37) T. Cool, H.K.D.H. Bhadeshia and D.J.C. MacKay, *Mater. Sci. Eng.*, **A233**, (1997), 186.

38) R. Lundberg, M. Waldenström and B. Uhrenius, *CALPHAD*, **1**, (1977), 97.

39) Metallurgical and Thermochemical Databank, National Physical Laboratory, Teddington, Middlessex, (1996).

40) M. Hillert and L.I. Staffansson, *Acta Chem. Scand*., **24**, (1970), 3618.

41) C. Zener, *Trans. AIME*, **167**, (1946), 513.

42) J.C. Fisher, *Trans. AIME*, **185**, (1949), 688.

43) H.K.D.H. Bhadeshia, *Metal Science*, **April**, (1981), 175.

44) H.K.D.H. Bhadeshia, *Metal Science*, **April**, (1981), 178.

45) J.R. Lacher, *Proc. Cambridge Philos. Soc*., **33**, (1937), 518.

46) R.H. Fowler and E.A. Guggenheim, Statistical Thermodynamics, Cambridge University Press, New York, (1939), 57.

47) G.Gosh and G.B. Olson, *Metall. Trans*., **7A**, (1976), 1897.

Table 1. Input variables of the Neural Network

Table 2. Fitting parameters estimated by non linear regression analysis to a $M_s = y_o + ax + by$ equation type

Table 3. Chemical composition of the six steels analysed.

Figure 1. Variation of (a) infered noise level (σ_V), and (b) test error (T_{en}) as a function of the number of hidden units.

Figure 2. Test error values of (a) the ten best Ms temperature models, and (b) the committee.

Figure 3. Comparison between the predicted and measured values of Ms for the training and test data using the 7 models committee.

Figure 4. Influence of C on Ms temperature.

Figure 5. Influence of (a) Mn, (b) Ni, and (c) Cu on Ms temperature

Figure 6. Influence of (a) Co, (b) W, (c) Mo, (d) Si and (e) Cr on Ms temperature.

Figure 7. Combined effect of (a) Ni-W, (b) Ni-Co, (c) Cr-W, and (e) Cr-Co on Ms temperature.

Figure 8. Effect of (a) Mn, (b) Ni, and (c) Cu on $\Delta G^{\gamma\alpha'}$ and $\Delta G_C^{\gamma\alpha'}$. Horizontal lines represent $\Delta G_C^{\gamma\alpha'}$.

Figure 9. Effect of (a) Co, (b) W, (c) Cr, (d) Si and (e) Mo on $\Delta G^{\gamma\alpha'}$ and $\Delta G_C^{\gamma\alpha'}$. Horizontal lines represent $\Delta G_C^{\gamma\alpha'}$.

Figure 10. Effect of Co in an alloy (a) without Cr, and (b) with Cr= 15wt.-%. Horizontal lines represent $\Delta G_C^{\gamma\alpha'}$.

Figure 11. Evolution of Ms as C and Cr concentrations varying from 0.001 to 0.9 wt.%, and from 0 to 17 wt.-%, respectively

Figure 12. Comparisson between results predicted by Equation (10), Andrews equation [6], Cool and Bhadeshia [36] model and Neural Network model.

Table 1. Input variables of the Neural Network

	Range (wt.-%)	Average (wt.-%)	Stardard deviation
C	0.001 – 1.62	0.3587	0.2044
Mn	0 – 3.76	0.8889	0.5258
Si	0 – 3.40	0.3434	0.4064
Cr	0 – 17.9	1.1824	2.4448
Ni	0 – 27.2	1.3792	3.8072
Mo	0 – 5.10	0.2984	0.5723
V	0 – 4.55	0.0727	0.2465
Co	0 – 30.0	0.4738	2.7788
Al	0 – 1.10	0.0115	0.0784
W	0 – 12.9	0.1108	0.8734
Cu	0 – 0.98	0.0498	0.1040
Nb	0 – 0.23	0.0016	0.0112
B	0 – 0.01	0.0020	0.0004
N	0.0001 – 0.06	0.0026	0.0088

Table 2. Fitting parameters estimated by non linear regression analysis to a

$M_s = y_o + ax + by$ **equation type**

	y_0	a	b	R
Ni	759,2159	-299,0917	-16,6297	0,99939313
W	770,8468	-312,8751	7,4229	0,99876925
Mo	769,8501	-306,0788	2,3693	0,99821097
Mn	768,4008	-301,4898	-30,6161	0,99812820
Cu	777,3075	-318,5246	-11,3436	0,99740703
Cr	759,5538	-290,7917	-8,9864	0,99832584
Si	769,8417	-311,3099	-14,4578	0,99867290
Co	738,6257	-281,2029	8,5810	0,98232872

Table 3. Chemical composition of the six steels analysed.

	C	Mn	Si	Cr	Ni	W	Co	Mo	V	Al	Cu	Nb	Ti
S1	0.45	0.4	0.32	13.0	0.38	0	0	0	0	0	0	0	0
S2	0.8	3.52	1.67	1.1	0	0.99	1.44	0.24	0	0.01	0	0	0
S3	0.07	1.5	0.37	0.039	0.49	0	0	0.021	0.004	0.045	0.039	0.03	0.01
S4	0.31	1.22	0.253	0.138	0.098	0	0	0.03	0.004	0	0	0	0
S5	0.09	1.03	0.16	9.1	0.99	0	0	0.99	0.19	0	0	0.04	0
S6	0.09	0.99	0.18	8.94	0	0.98	1.87	0.96	0.18	1.87	0	0.05	0

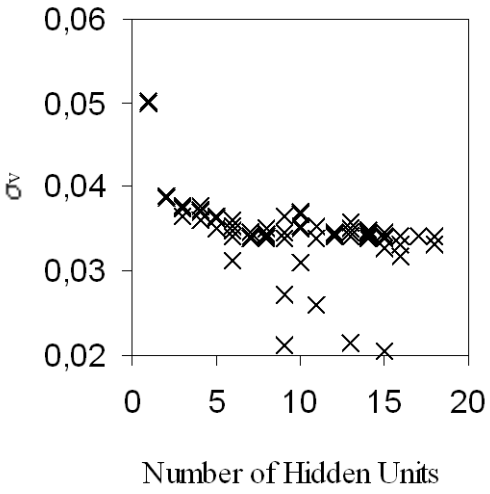

(a)

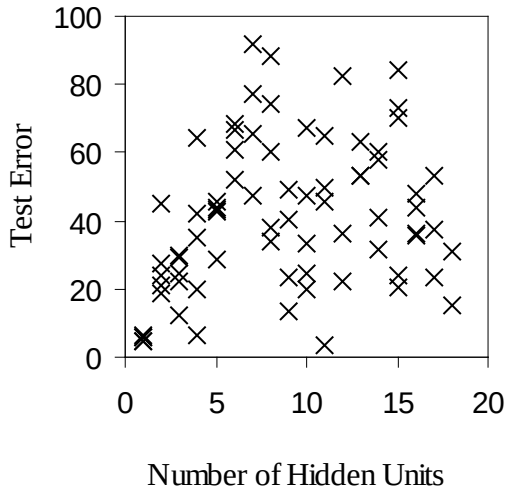

(b)

Figure 1. Variation of (a) infered noise level (σ_V), and (b) test error (T_{en}) as a function of the number of hidden units.

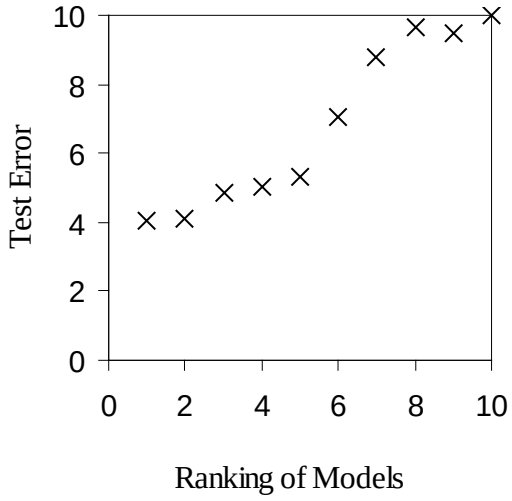

(a)

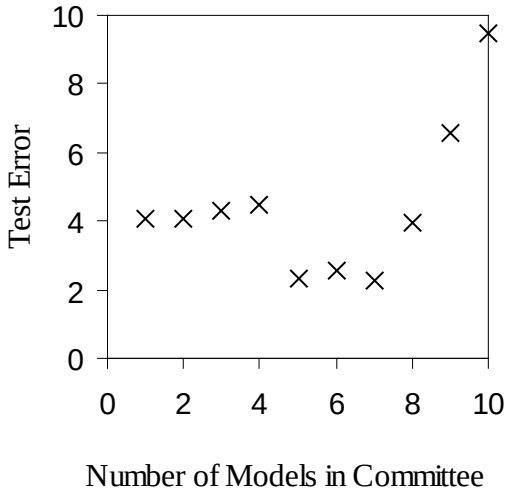

(b)

Figure 2. Test error values of (a) the ten best Ms temperature models, and (b) the committee.

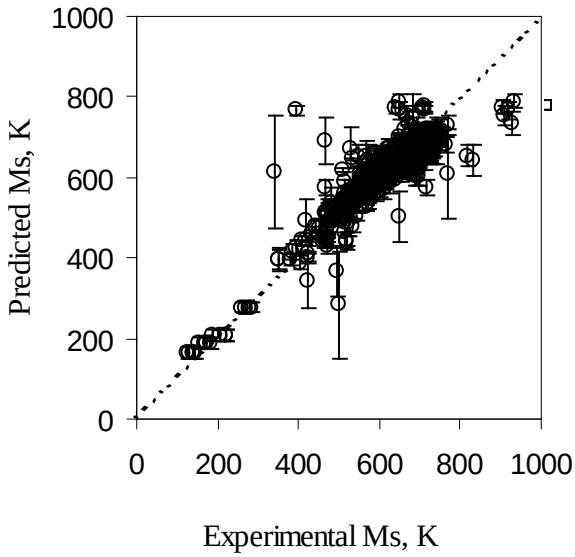

Figure 3. Comparison between the predicted and measured values of Ms for the training and test data using the 7 models committee.

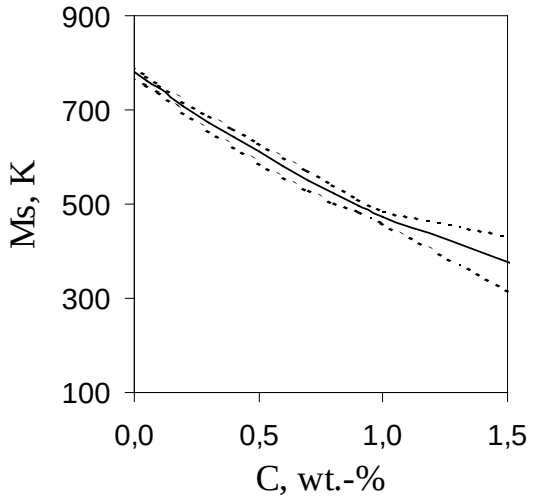

Figure 4. Influence of C on Ms temperature.

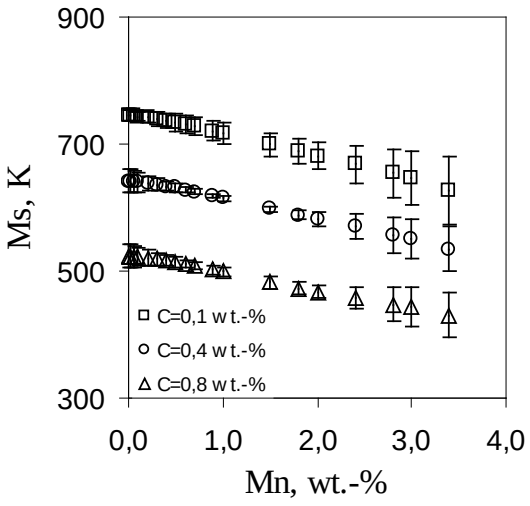

(a)

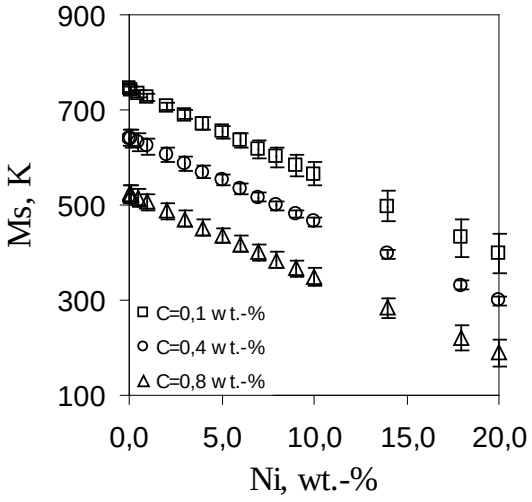

(b)

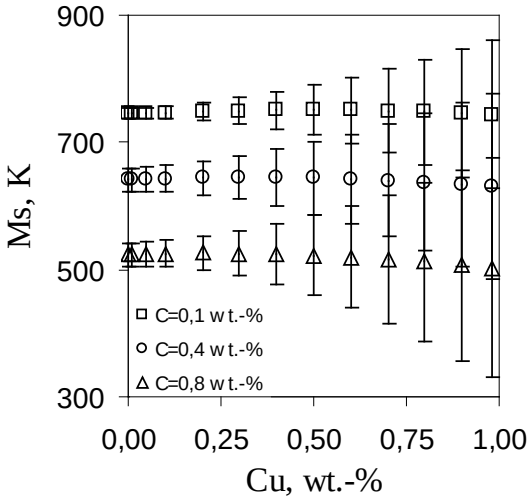

(c)

Figure 5. Influence of (a) Mn, (b) Ni, and (c) Cu on Ms temperature

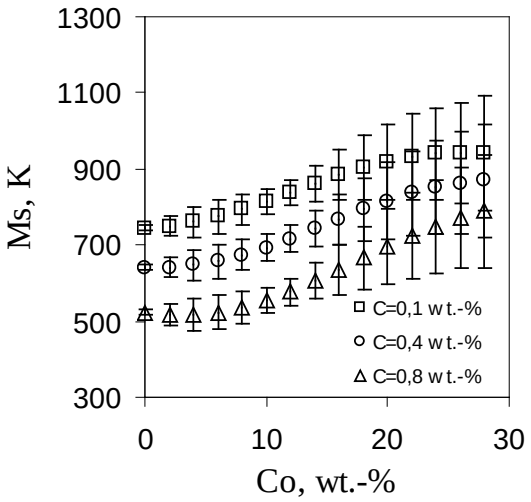

(a)

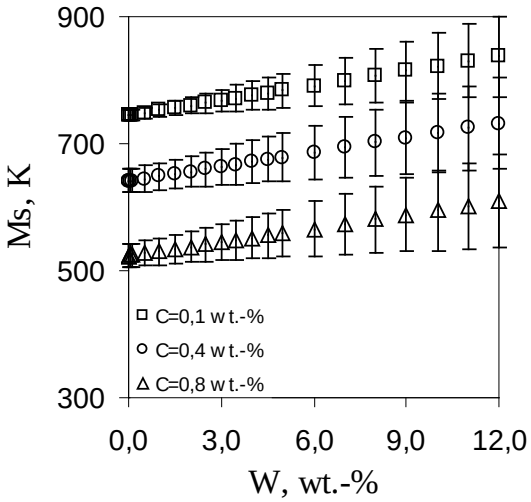

(b)

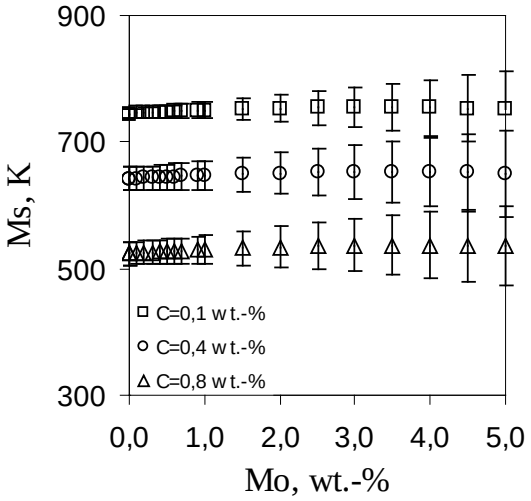

(c)

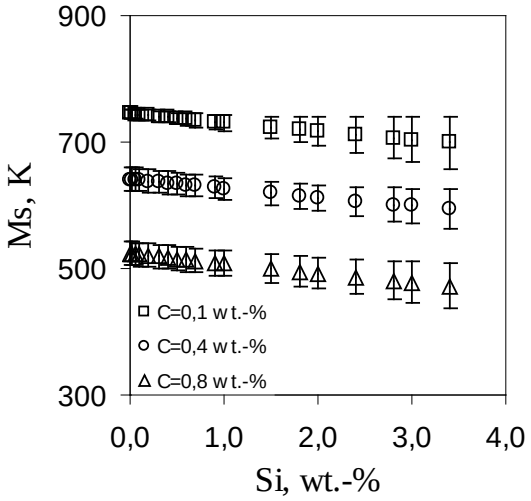

(d)

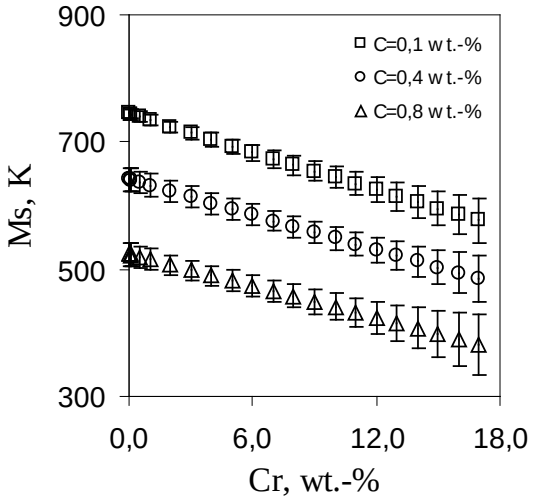

(e)

Figure 6. Influence of (a) Co, (b) W, (c) Mo, (d) Si and (e) Cr on Ms temperature.

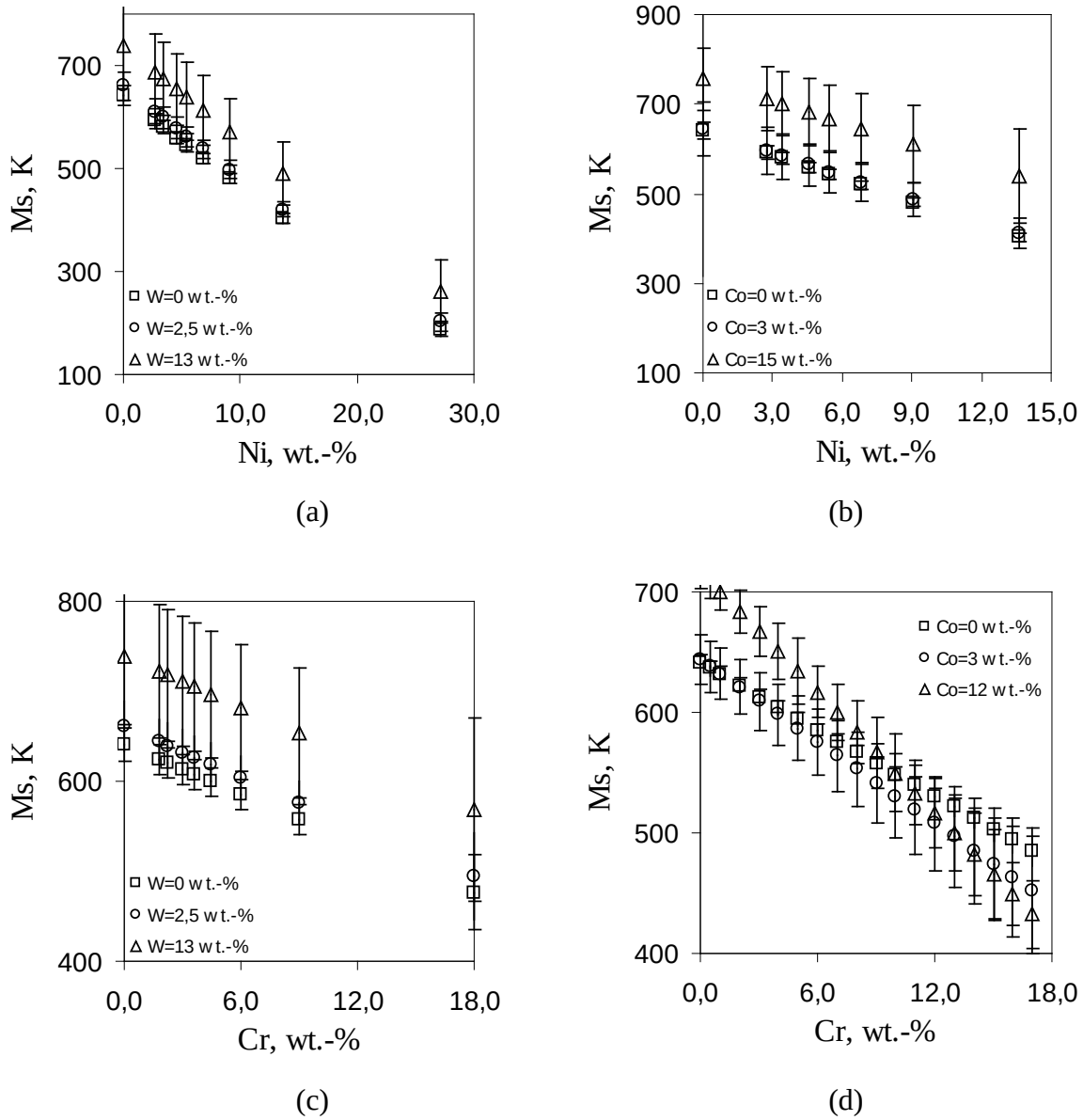

Figure 7. Combined effect of (a) Ni-W, (b) Ni-Co, (c) Cr-W, and (e) Cr-Co on Ms temperature.

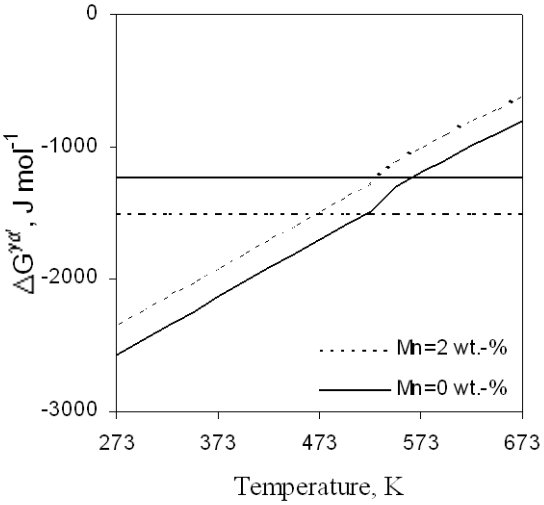

(a)

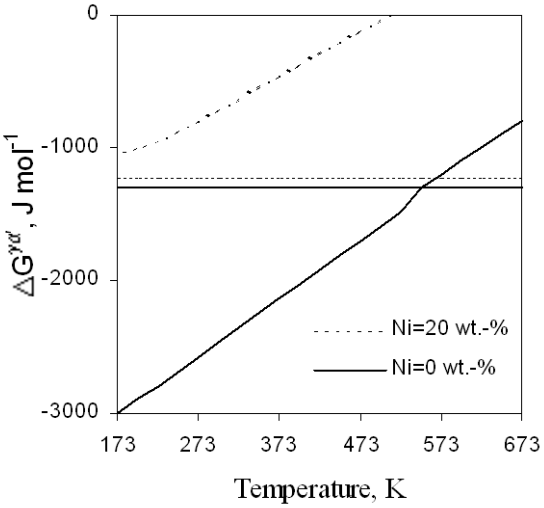

(b)

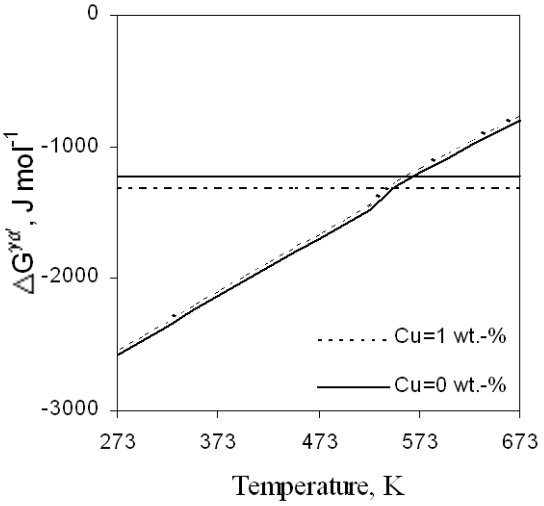

(c)

Figure 8. Effect of (a) Mn, (b) Ni, and (c) Cu on $\Delta G^{\gamma\alpha'}$ and $\Delta G_C^{\gamma\alpha'}$. Horizontal lines represent $\Delta G_C^{\gamma\alpha'}$.

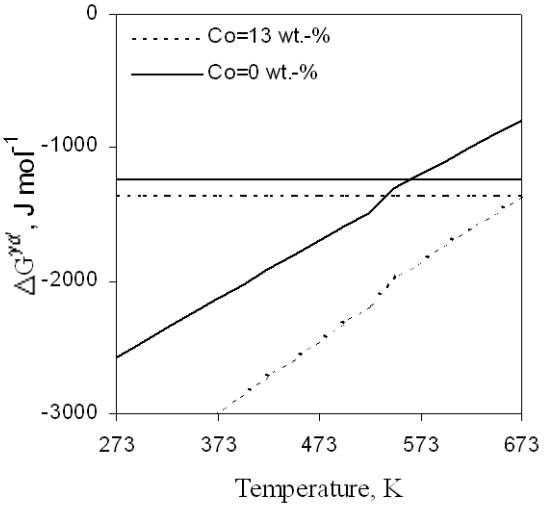

(a)

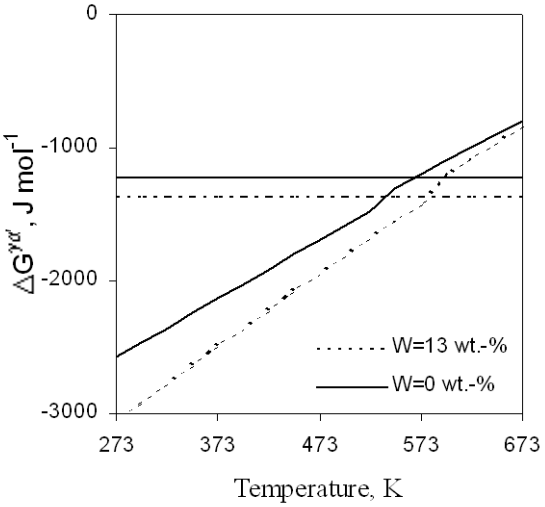

(b)

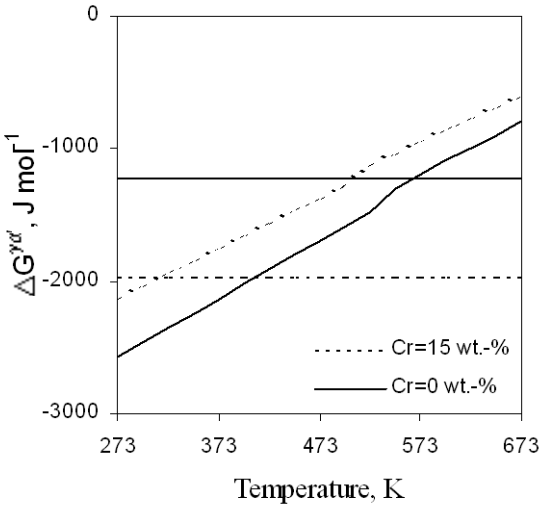

(c)

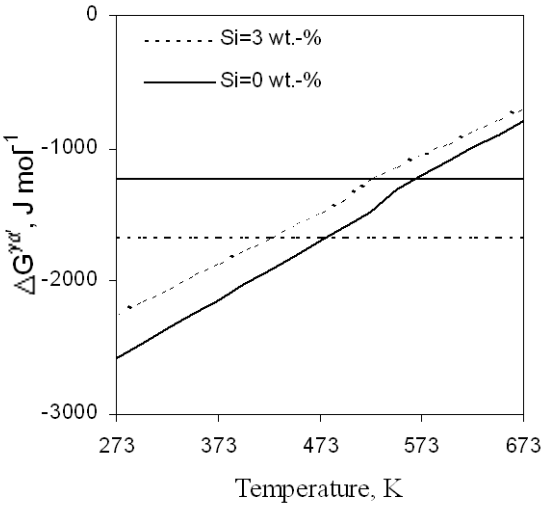

(d)

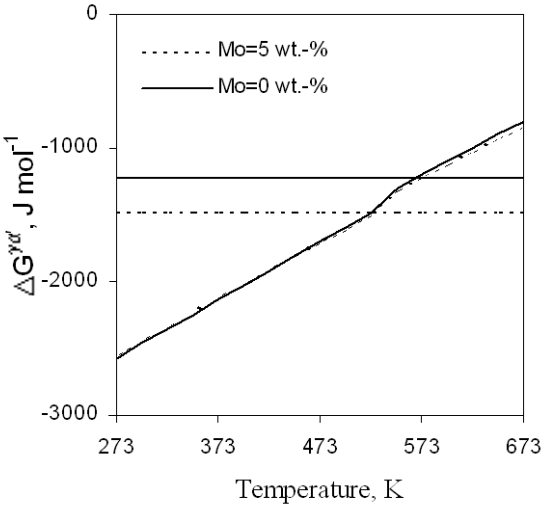

(e)

Figure 9. Effect of (a) Co, (b) W, (c) Cr, (d) Si and (e) Mo on $\Delta G^{\gamma\alpha'}$ and $\Delta G_C^{\gamma\alpha'}$. Horizontal lines represent $\Delta G_C^{\gamma\alpha'}$.

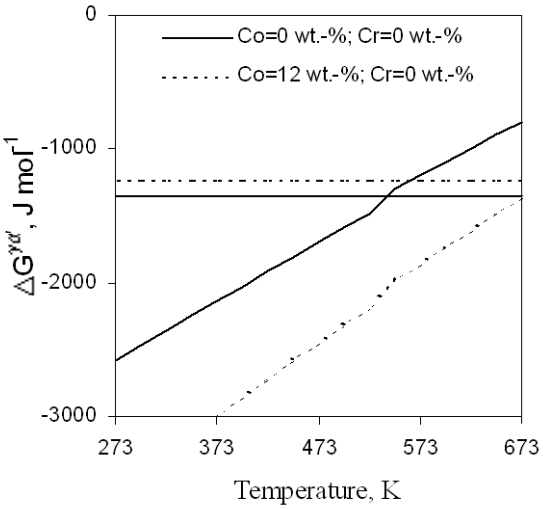

(a)

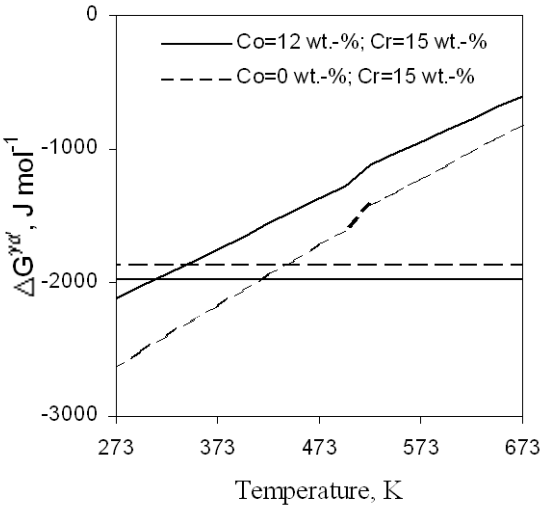

(b)

Figure 10. Effect of Co in an alloy (a) without Cr, and (b) with Cr= 15wt.-%. Horizontal lines represent $\Delta G_C^{\gamma\alpha'}$.

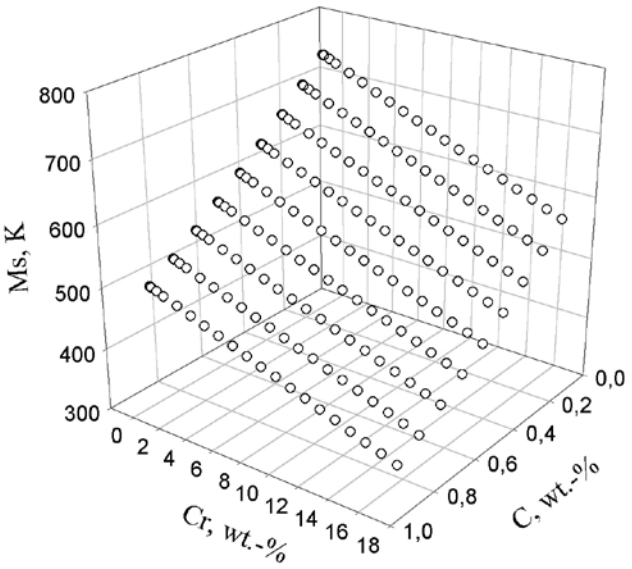

Figure 11. Evolution of Ms as C and Cr concentrations varying from 0.001 to 0.9 wt.%, and from 0 to 17 wt.-%, respectively

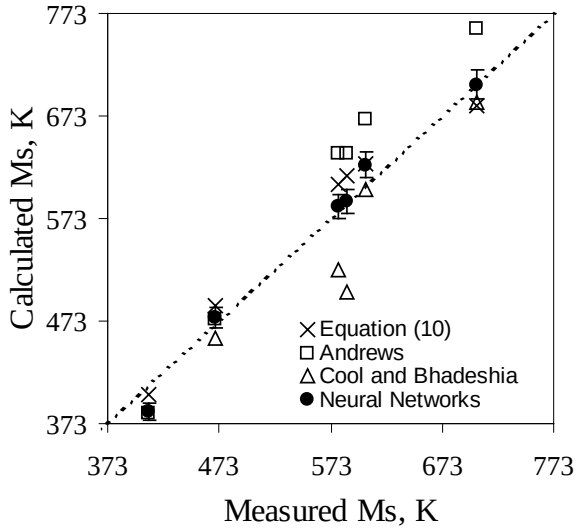

Figure 12. Comparisson between results predicted by Equation (10), Andrews equation [6], Cool and Bhadeshia [36] model and Neural Network model.